

Electron Microscopy and Microanalysis of Ceramics

Gareth Thomas

Department of Materials Science and Mineral Engineering, University of California, Berkeley, CA 94720-1760, USA;
and Materials Sciences Division, Lawrence Berkeley Laboratory, 1 Cyclotron Road, Berkeley, CA 94720, USA

(Received 1 June 1995; revised version received 22 June 1995; accepted 28 June 1995)

Abstract

We live and work in a world that depends on materials and their performance. The science of materials has developed to a position of great understanding, such that materials can be microscopically tailored to provide specific sets of properties. The practical applications of newly designed materials depend on market interest and costs. In the final analysis it is the processing of materials that remains the key factor. In order to facilitate technical advances, the relationships between processing, microstructure, and performance must be established. This task is generic to all materials whether for mechanical or physical property goals. Central to such understanding is the role played by electron optical, diffraction and analytical methods of characterization in their specificity to synthesis almost to the atomic level.^{1–3} This paper provides some examples of such applications to several ceramic systems, and attempts to indicate the generic nature of many problems to be solved.

1 Introduction

Materials science is concerned with the understanding of the relationships between *processing–structure–properties* as shown schematically in Fig. 1(a). Electron microscopy, diffraction and microanalysis are especially important for characterizing materials because of their specificity and high spatial resolution, as is now very well known. In the last decade or so the number of investigations using these techniques for characterizing ceramics has increased greatly and many examples of such are in the ceramics and electron microscopy literature.⁴

There is a wealth of information about structure, microstructure, chemical composition, etc., obtainable from state-of-the-art instruments as indicated in Fig. 1(b). It is clear that no materials research laboratory can function properly without such facilities.

In this paper no attempt will be made to review the vast field of applications to ceramics. Instead, some general points will be discussed relevant to electron imaging, diffraction and spectroscopy techniques, and the paper will be illustrated by representative examples, mostly drawn from research programs at U.C. Berkeley.

2 General Remarks

2.1 Interpretation of results: resolution

While excellent commercial microscopes are now generally available with capabilities of better than 2 Å interpretable resolution, and which provide data as is illustrated in Fig. 1(b), a word of caution is needed. With a good thin specimen it is relatively easy to obtain excellent images, diffraction and spectroscopic data. However, the *interpretation*, especially, of high resolution images *must* be done with the appropriate matching calculations.² As shown in Fig. 2, structure images are very sensitive to microscope conditions, especially objective lens defocus and specimen thickness.³ Thus, the materials scientist must know the instrumental conditions from source to image recording in order to sensibly utilize the images. Without calculations, publications of micrographs are, to put it bluntly, almost useless. In fact it is necessary to interpret all the data with suitable computer simulations/calculations. Programs for these purposes are available from several laboratories.⁵

When instruments, specimens and simulations are optimized and effectively used, then electron microscopy becomes a unique tool. For example, it is possible to do structure analysis on nanocrystals in real space from images in different orientations. Figure 3 is an example for mullite.³ Clearly, large-angle tilt specimen holders ($\pm 45^\circ$) are a necessity with the requirement to maintain the resolution over the complete tilt range. A clear application of such work is in the analysis of nanostructures or small second phases which

Materials Science Iterative Tetrahedron

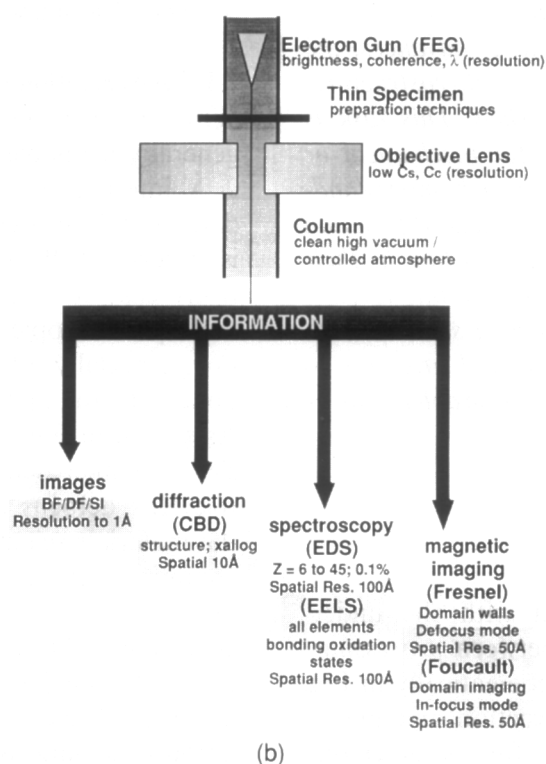
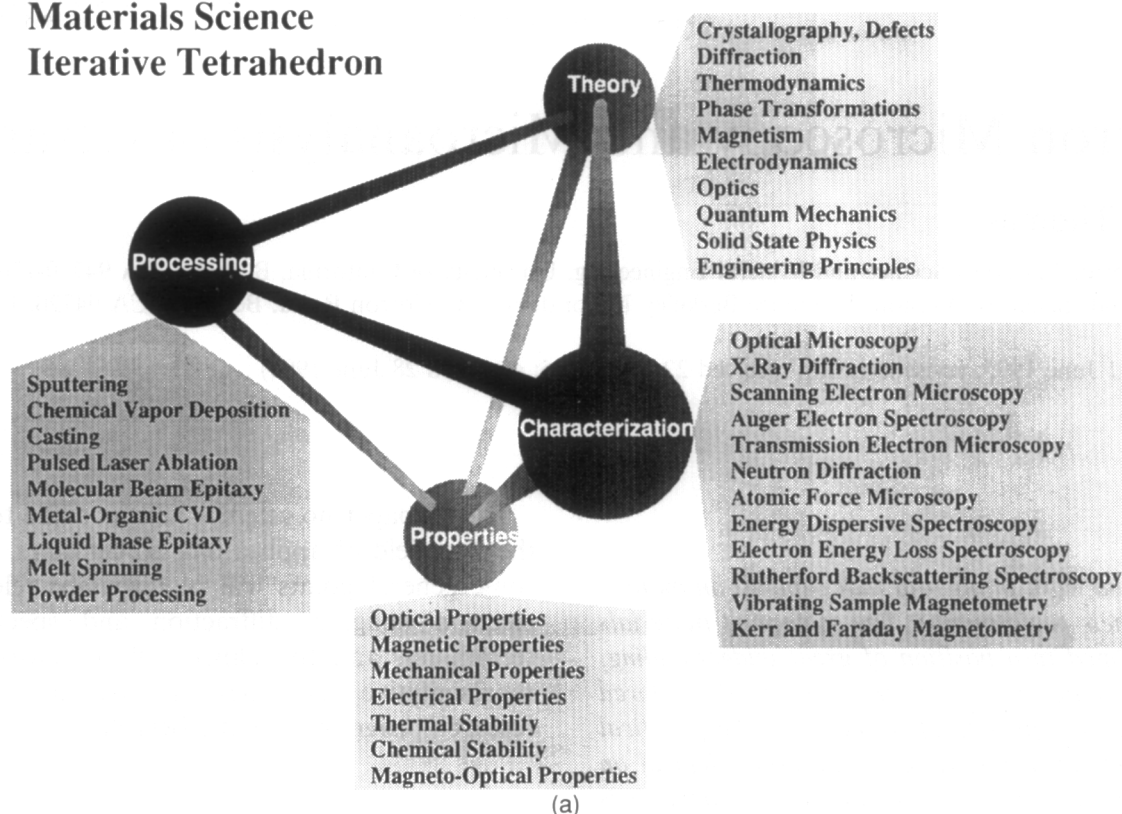


Fig. 1. (a) Scheme showing the iterations involved in materials science and engineering research. (b) Schematic showing the wide range of high resolution information available from modern electron optical facilities.

would not be amenable to traditional X-ray studies.

The question of resolution is very important for ceramics. Until recently, instruments did not have the resolution capable of interpreting the positions of small anions in structures; and to increase resolution by lowering the wavelength (raising voltage) increases the probability of displacement radiation damage. Consequently, a new generation of high

resolution (HREM) instruments are now becoming available at moderate voltages (300–400 kV), by developing low aberration objective lenses (operated with large magnetic fields) and/or incorporating holographic capabilities. In addition, and essential for improved analytical resolution, intense coherent electron sources by field emission are finally becoming generally available. Figure 4, using essentially a weak phase object analysis,

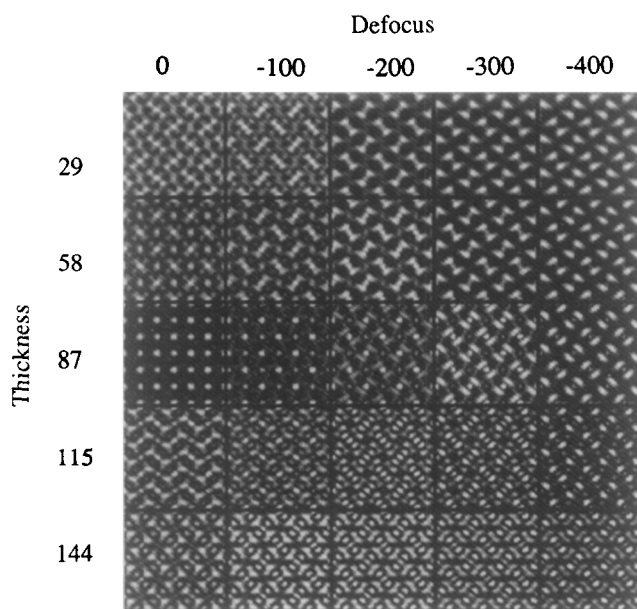


Fig. 2. 001 projected images computed for mullite $3\text{Al}_2\text{O}_3 \cdot 2\text{SiO}_2$ as a function of specimen thickness and objective lens defocus. Experimental images must match these conditions to be interpretable (Ref. 3).

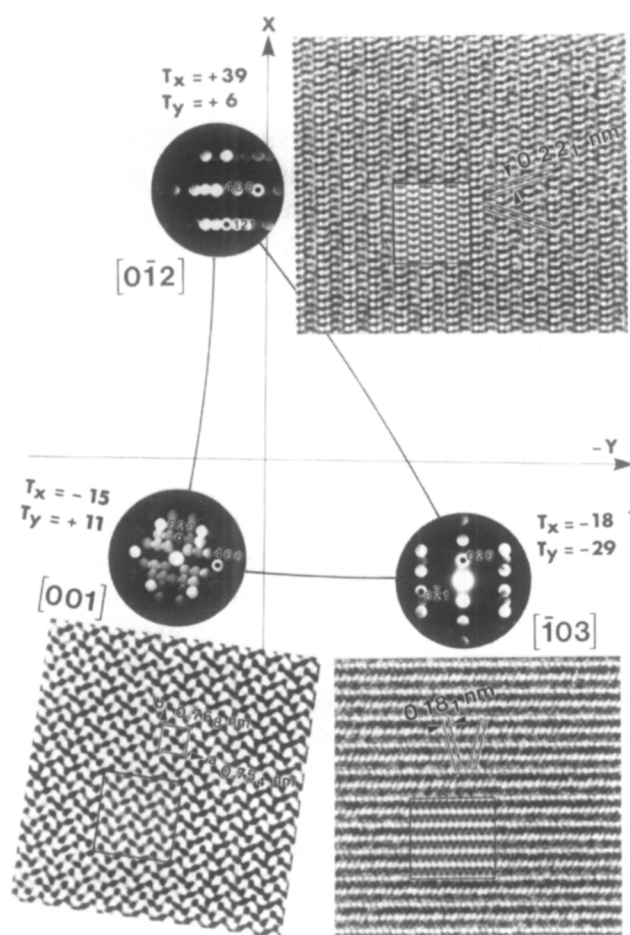


Fig. 3. Structure images obtained in the Berkeley ARM microscope for a crystal of mullite. Three different orientations allow the orthorhombic structure to be verified when images match simulations (inset rectangles). Point-to-point resolution is 1.6 \AA (courtesy T. Epicier).

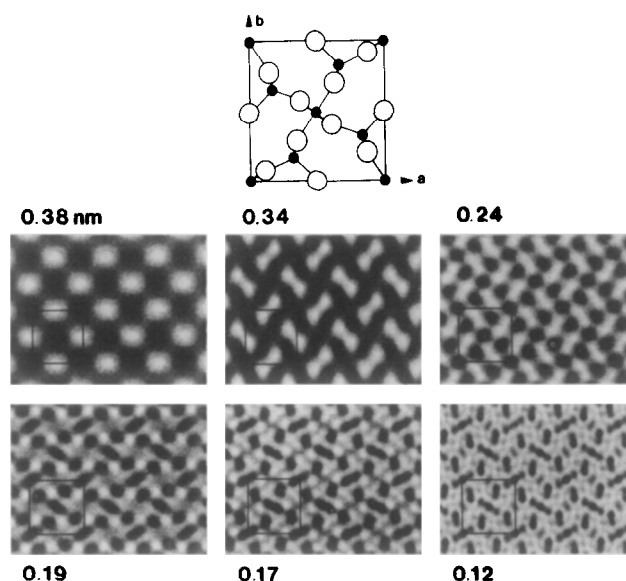


Fig. 4. Simulations of the 1.2 \AA resolution required to distinguish oxygen from the Al, Si cations in the [001] projection of orthorhombic mullite (courtesy M. O'Keefe).

shows that an instrument of resolution better than 1.2 \AA is needed to distinguish oxygen in the 001 projection of mullite. Such instrument development allows materials scientists to probe materials at or near atomic levels. Image information at 1 \AA is now possible with computer-assisted deconvolution of sequential recording, e.g. the work at Antwerp (G. Van Tendeloo, reported at this session).

However, electron microscopy is not only a problem of instrumental resolution and interpretation, it is also a problem of specimen preparation. For example, glasses and glassy films are very important in ceramics, as will be illustrated below. In order to resolve the structure of even a simple SiO_2 glass, assuming a random network, Fig. 5 indicates the specimen must be less than 10 \AA thick, and this is obviously a terrible restriction.

2.2 Convergent beam diffraction (CBD)

This diffraction method probes the three-dimensional structure (Fig. 1) providing three-dimensional reciprocal space data which in turn allow the researcher to fix the crystal structure and point/space symmetries.⁶ The development of convergent beam diffraction, which is a powerful analytical technique, has enabled detailed crystallographic analyses to be done on nanostructured materials and within very small volumes. In addition, high resolution analyses of large-angle lines in the patterns allow very accurate lattice parameter measurements to be made. Typical applications include studies of phases, e.g. the so-called morphotropic boundary in ferroelectric systems such as lead zirconate titanate,⁷ indicate that both the rhombohedral and tetragonal phases exist over a very narrow composition range, so that the

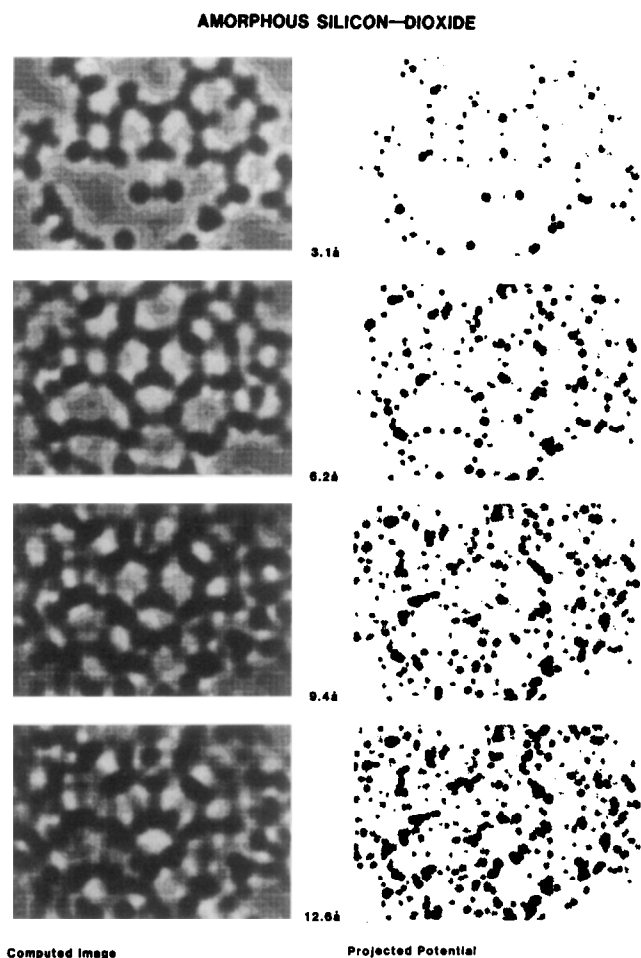


Fig. 5. Random network model of SiO_2 glass showing projected potentials and corresponding image simulations. Notice that the images become very difficult to interpret when the specimen is ≥ 10 Å thick (courtesy M. O'Keefe).

'phase diagram' normally utilized is not correct. In another application the CBD method has been essential in helping to analyze the oxygen problem in AlN, as has been published recently.⁸ In this system spectroscopic analyses are confused because of the presence of surface oxide films, so that CBD seems the only way to probe the oxygen content and its variability from grain to grain and at/across grain boundaries. However, this can be achieved only when the relationship between lattice parameter and (dissolved) oxygen has already been established, and the appropriate computer simulations have been carried out to interpret the CBD measurements. This particular case illustrates that problem solving should involve utilization of all the available techniques⁹ and not just any one technique.

Ceramic materials are generally more complex than metallic systems and often have low crystal symmetries. Mullite close to $3\text{Al}_2\text{O}_3:2\text{SiO}_2$ is orthorhombic, yet when prepared as whiskers can also occur in the metastable tetragonal structure.¹⁰ Such discoveries would not be possible without analytical techniques, such as CBD, capable of

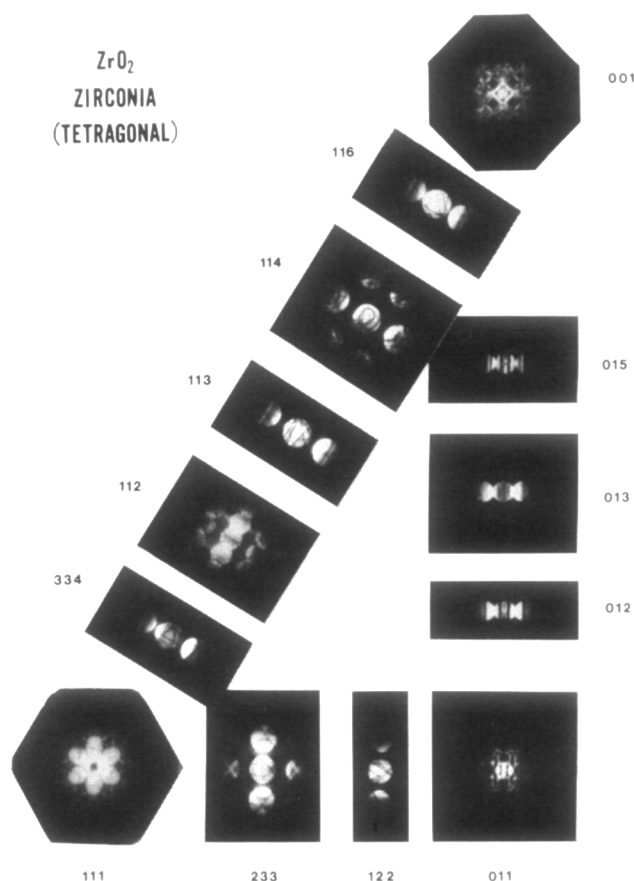


Fig. 6. CBD reciprocal space map for tetragonal ZrO_2 . Such maps are useful for structure analysis, orientation determination, and general crystallographic data.

resolving small sized materials — whiskers in this case. In combinations of large tilt angles the full crystal structure-orientation can be represented as CBD (or Kikuchi) maps.⁹ An example for tetragonal ZrO_2 is shown in Fig. 6. Such maps can also be simulated by using the appropriate computing software. These maps are also useful for controlling the orientation for many situations, e.g. selecting the correct diffraction conditions for high resolution imaging,² contrast analyses,⁹ lattice parameter or strain measurements, etc.⁶ Due to the complexity of diffraction problems arising from multiple scattering in low symmetry structures and orientations, it becomes almost impossible to recognize spot diffraction patterns except for the simplest cases. It is thus recommended to use microdiffraction (CBD) or thick specimen Kikuchi maps to assist the investigator in correctly assessing the appropriate diffraction conditions.⁹

2.3 Contrast analyses: defects

Defect analysis is important but often difficult due to the reasons given above. In amplitude contrast analysis the contrast depends on the phase factor $2\pi\vec{g} \cdot \vec{R}$ where \vec{g} is the operating diffraction vector and \vec{R} is the displacement vector.⁹ \vec{R} can be quite complex, especially in non-isotropic systems. Also, the magnitude of $\vec{g} \cdot \vec{R}$, which must shift the inten-

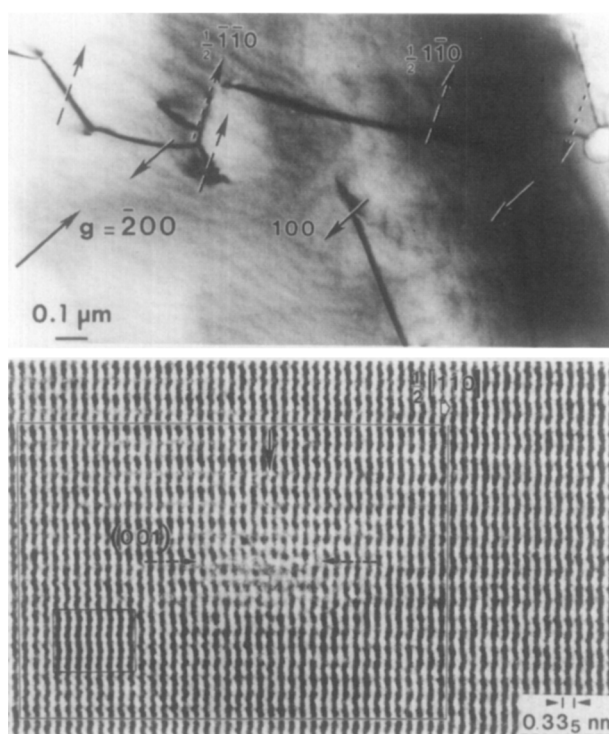


Fig. 7. AlTiO_5 : Simplified Bravais lattice showing shortest translation vectors. Top RH: amplitude contrast image to set dislocations with $\vec{b} = \frac{1}{2}\langle 001 \rangle$ invisible. Lower RH: structure imaging-closure circuit shows $\vec{b} = \frac{1}{2}\langle 001 \rangle$ directly (Ref. 11).

sity by at least $\pm 10\%$ over background for visibility, may be too small to evaluate \vec{R} , (e.g. for interface dislocations whose \vec{R} vector may be \ll lattice vectors). In general, dislocations in crystals

are expected to be those of smallest Burgers vectors (lowest energies). Figure 7 is an example of dislocation Burgers vector analysis in AlTiO_5 ¹¹ (space group Cmc2, $a = 0.35$ nm, $b = 0.94$ nm, $c = 0.96$ nm), in which the simplified Bravais lattice indicates the expected Burgers vectors to be the shortest vectors in the close-packed planes ($a < b < c$). One of several $\vec{g} \cdot \vec{b}$ conditions is shown, alongside a structure image. The analysis of Burgers vectors and habit planes is consistent with elementary crystallographic considerations: $[100]$ and $\frac{1}{2}[110]$ -type translation vectors are the shorter ones (0.36 and 0.53 nm respectively), and (011) and (001) are two of the densest planes; these planes are probably glide planes. The HREM approach is very useful when $(\vec{g} \cdot \vec{R})$ is very small (dislocations not visible), and can be effectively used in studying defects and structural aspects of interfaces and grain boundaries which contain structural defects with displacements not equal to the lattice vectors.

Many other examples of defect analysis could be given, but space is limited. Therefore, we mention just one other case for planar faults which have importance in several technically important ceramics, e.g. nitrogen ceramics,¹²⁻¹⁴ superconductors,¹⁵ minerals, etc. These are the 'composition' faults which occur to adjust to compositional changes, and are properly described as polytypoids—to be distinguished from polytypic faults which affect structure but not composition (SiC is

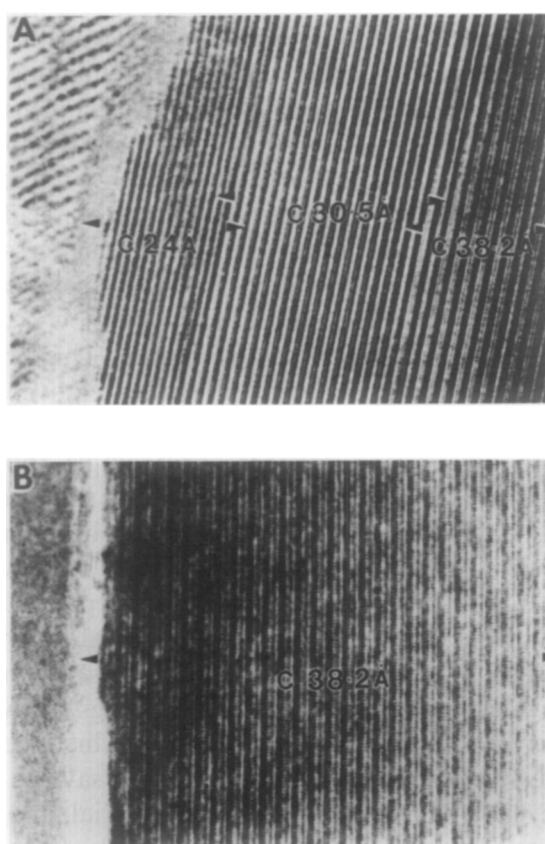


Fig. 8. Showing polytypoids near grain boundary in alkaline earth superconductors; caption as indicated.

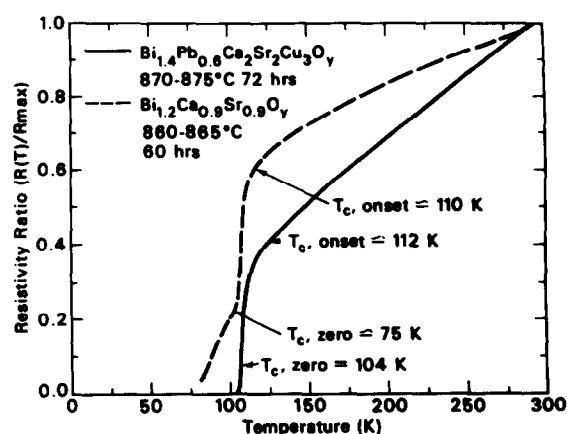


Figure (above)
Plot of resistivity versus temperature for loaded (—) and the unloaded (---) samples of Bi-containing superconducting materials. Note the presence of a step in the resistivity plot for the unloaded sample resulting in a lower T_c . (XBL 884-7341)

Figure (above, left)
High resolution lattice fringe electron micrograph of the unloaded sample showing the decrease in c -parameter close to the grain boundary. The 24 Å spacing polytypoid has a T_c of 20 K, the 30.5 Å polytypoid a T_c of 75 K and the 38.2 Å polytypoid a T_c of 110 K.

Figure (left)
High resolution lattice fringe image from the loaded sample showing the uniform c -parameter of 38.2 Å up to the grain boundary.

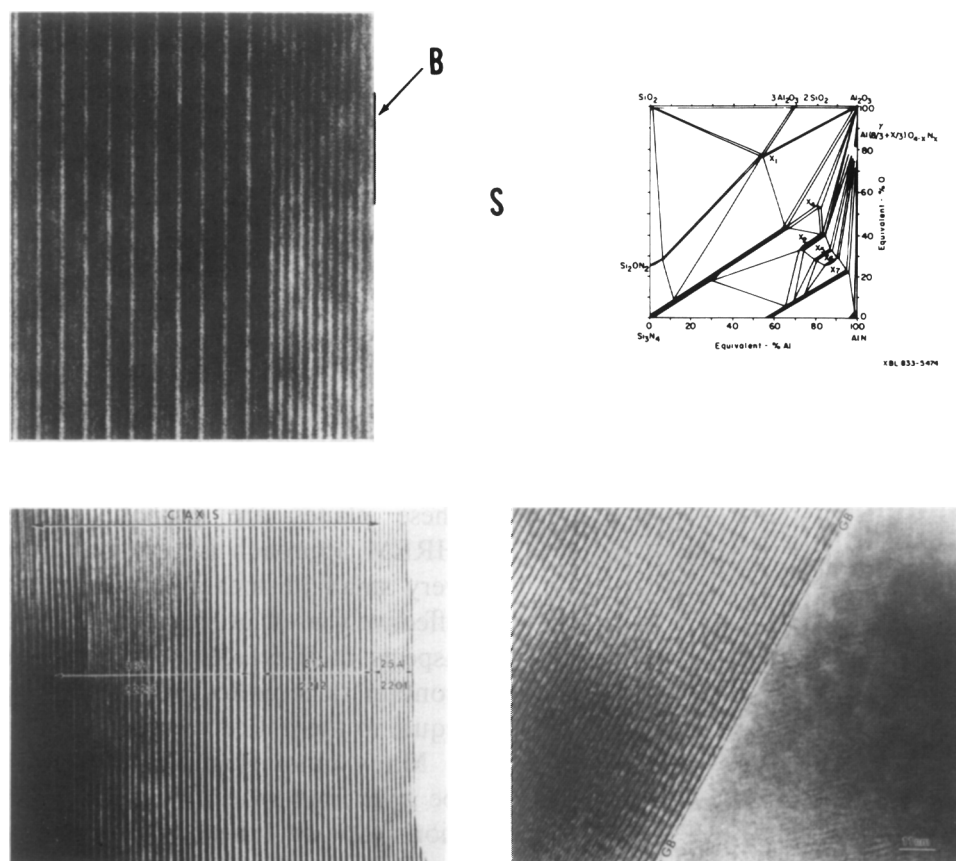


Fig. 9. Polytypoids in MgSiAlON and a section of the phase diagram; due to composition changes (Mg/Si ratios) the polytypoid spacing changes: each $|c|$ axis parameter corresponds to a unique composition and thus indirectly provides compositional data (courtesy D. R. Clarke).

a well known example). In the electron microscope, such polytypoids can be considered as projections of compositional images, as each structure has a unique cation: anion ratio.

In superconductors the faulting associated with Cu–O layers has a strong effect on physical properties, especially the critical temperature. Compositional changes near grain boundaries can locally generate polytypoids of low T_c , as shown in Fig. 8. Suitable sintering aids (in this case PbO) can alleviate these structural problems and hence reduce the problem of grain boundary resistivity and lack of connectivity. This example typifies the need to closely monitor processing–microstructure relationships. Shown for comparison to Fig. 8 is Fig. 9, with similar structural polytypoids due to changes in Mg/Si/O ratios in MgSiAlON ‘alloys.’

2.4 High voltage TEM — penetration

HVEM (>300 kV) is useful not only because of improved resolution (shorter wavelength) and reduced ionization damage (but increased knock-on damage for voltages $>$ threshold), but also for increased penetration up to 1 meV.⁹ The latter benefit is useful in dealing with complex materials such as composites, coated fibres, etc. in which specimen thinning for 200 kV transparency is particularly difficult.¹⁶

An example is that for BN coated fibres. Preparation of TEM specimens of composite materials can be complicated by the mere fact of the existence of two or more different phases in the material. For instance, ion-beam thinning can preferentially remove one phase if it happens to be softer than the other. In the case of SiC fiber/SiC matrix specimens, the fiber–matrix interface has been deliberately engineered to be weak, leading to a material with improved fracture toughness. This leads to difficulty in preparing thin specimens for TEM, as the fibers tend to fall out below a certain thickness, leading to sample failure. This problem has been circumvented by preparing relatively thick specimens of the composite and observing them at high accelerating voltages. The sample shown in Fig. 10 was observed at 1500 kV. It shows clearly the circumferential cracking in the boron nitride coating on the fiber. Such cracking increases the energy of propagation of a crack perpendicular to the fibers, leading to improved material toughness.

The use of ceramic components in turbine engines could lead to weight savings as well as increases in operating temperature, which increases fuel efficiency. The potential dollar savings could be enormous. One candidate material, molybdenum disilicide,¹⁷ has relatively high creep rates above 1000°C. A possible solution is to use a rein-

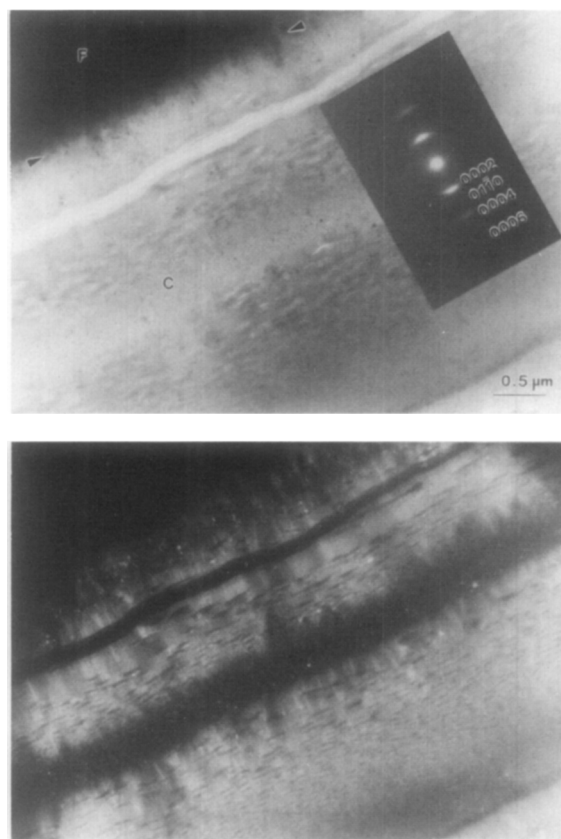


Fig. 10 Bright field (a) and dark field (b) pair of TEM micrographs showing circumferential crack (labeled 'C') in BN coating of SiC fiber in ceramic composite. Cracking in the coating increases the composite toughness. Imaging at 1500 kV (courtesy A. McFayden).

forcement with a very low creep rate, in this case mullite.¹⁸ Improvement in creep performance depends upon the formation of a strong interface between the two materials. Diffuse dark field imaging, shown in Fig. 11, indicates the presence of a small amount of glassy phase at the interface prior to creep deformation. Current experiments indicate increased creep resistance, implying a change in the interphase glass—possibly devitrification. Clearly crept specimens will be examined carefully by HREM and AEM to investigate this interesting situation.

2.5 Microanalyses

Figure 1 also illustrates the information available by microanalysis (AEM). AEM is now a widely accepted technique.¹⁹ X-ray spectroscopy spatial resolutions of 10 nm capable of identifying elements from $Z = 6$ to $Z = 60$ by EDS have become almost routine. Detection limits are about 0.1% with field emission sources, depending on the signal-to-noise ratio, detector efficiency, and data retrieval from small volumes. Again, it should be pointed out that intense sources, (e.g. FEG) can give rise to problems such as heating, radiation damage and even decomposition, such as loss of nitrogen from nitride ceramics.

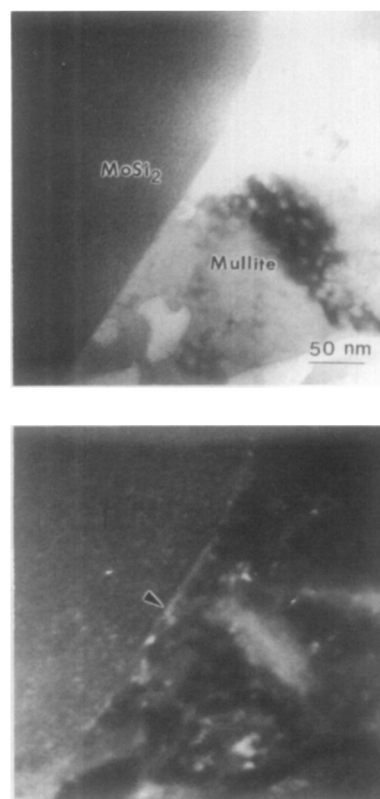


Fig. 11. Bright field (a) and diffuse-dark field (b) pair of TEM micrographs showing glassy layer (arrow) between MoSi_2 and mullite phases in ceramic composite. The creep resistance of the composite is dependent on the morphology and composition of this layer. Imaging at 120 kV (courtesy A. McFayden).

Energy loss spectroscopy, EELS, is also progressing mainly as a qualitative method useful for light elements, and should be used more widely, especially coupled with high resolution imaging studies of ceramics. It is also very effective in analyzing bonding relationships from details of the fine structure near the absorption edge. It is possible to detect graphite with diamond in 50 Å particles,²⁰ as shown in Fig. 12. With image analysis it is a very powerful addition to the battery of electron optical techniques available in modern microscopes.

2.6 Magnetic structure

Magnetic structure and properties also depend on microstructure and local composition. Examples include domain wall pinning of soft ferrites, which raises coercivity but lowers permeability. The problem with magnetic imaging is that to obtain high resolution, one needs objective lenses of low aberrations. This means working at very high magnetic fields in the objective, e.g. up to 2 or more Tesla. Such fields saturate magnetic specimens in the microscope, rendering them useless for magnetic structure imaging. Thus, unless special instruments are available for observing specimens in zero field environments, one is restricted to turning off the objective lens, so limiting observation to

Spatial Resolution

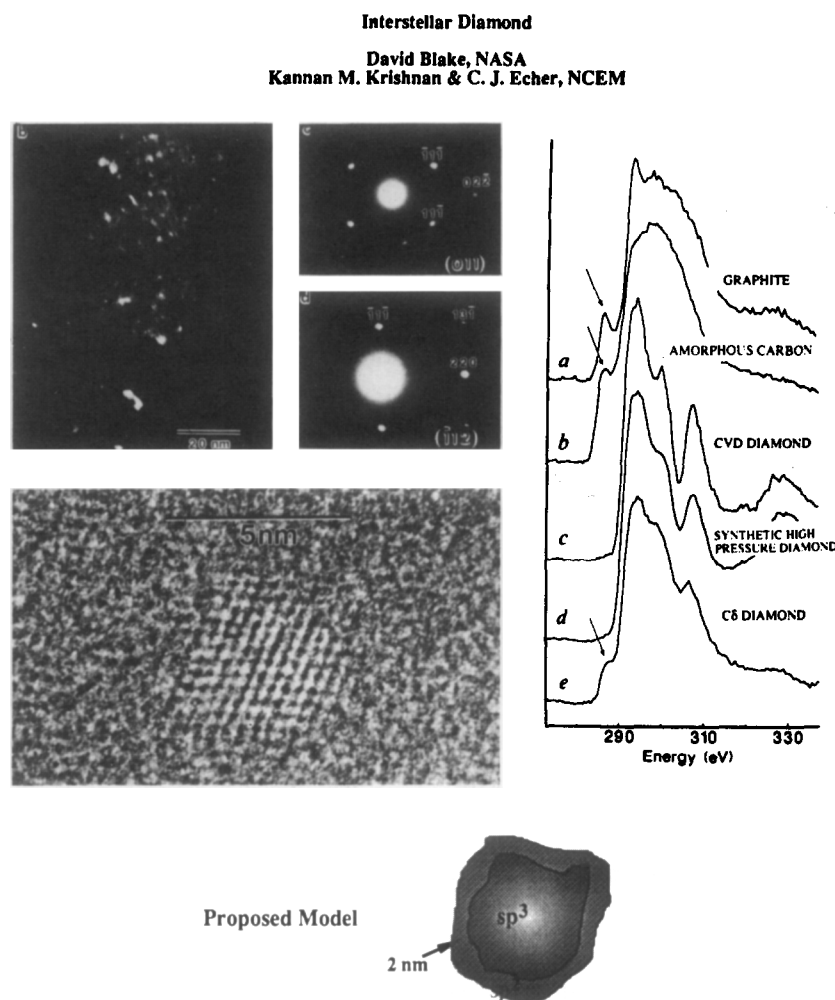


Fig. 12. EELS studies of nanocrystalline meteoric diamond. The HREM lower left dark field image shows the small particles of meteoric diamond. The EELS spectra on the RH side are from carbon phases near the absorption edge (K). The sp_2 graphite transition can be seen in the C δ spectrum from the diamond particle shown. It is concluded that the diamonds are coated with a graphite layer (Ref. 20). (Courtesy K. Krishnan.)

low-resolution Lorentz imaging.^{9,21} If, however, a high voltage instrument is available with free lens control, it is possible to obtain 10 nm or less resolution, as has been demonstrated recently in our laboratory. Figure 13 shows an example of such research, in which particles of Co, some being single-domain at <100 nm diameter, are magnetically imaged in a gold matrix. The size and morphology of these Co particles have a major effect on giant magnetoresistance and this effect is of great interest for magnetic recording. For soft ferrites, Fig. 14 is an example of low resolution 'conventional' imaging of domain walls, which indicates the pinning power of grain boundaries on the domain walls in Mn/Zn ferrites.²² Microanalyses by AEM and CBED proved that such pinning is associated with CaO impurity segregation and its associated lattice distortion, and results in poor permeability properties. This result again shows the importance of material purity and processing on microstructure-property relationships.

3 Representative Examples

Representative examples of the use of electron microscopy in ceramics can be drawn from the tremendously important problem of grain boundaries, interfaces, and interphase interfaces,²³ as many examples will be given in this symposium. Grain boundary engineering is quite generic and is required to control many mechanical and physical properties. Figure 15 is a schematic to illustrate this point and Fig. 8 is one example for electronic conduction in superconductors.

3.1 Properties and intergranular phases: Si_3N_4

In the case of many ceramics whose bonding characteristics require the use of sintering aids to achieve densification, the resulting materials often contain residual, glassy phases at grain boundaries (Fig. 15). Silicon nitride is a typical example. These amorphous phases, depending on their composi-

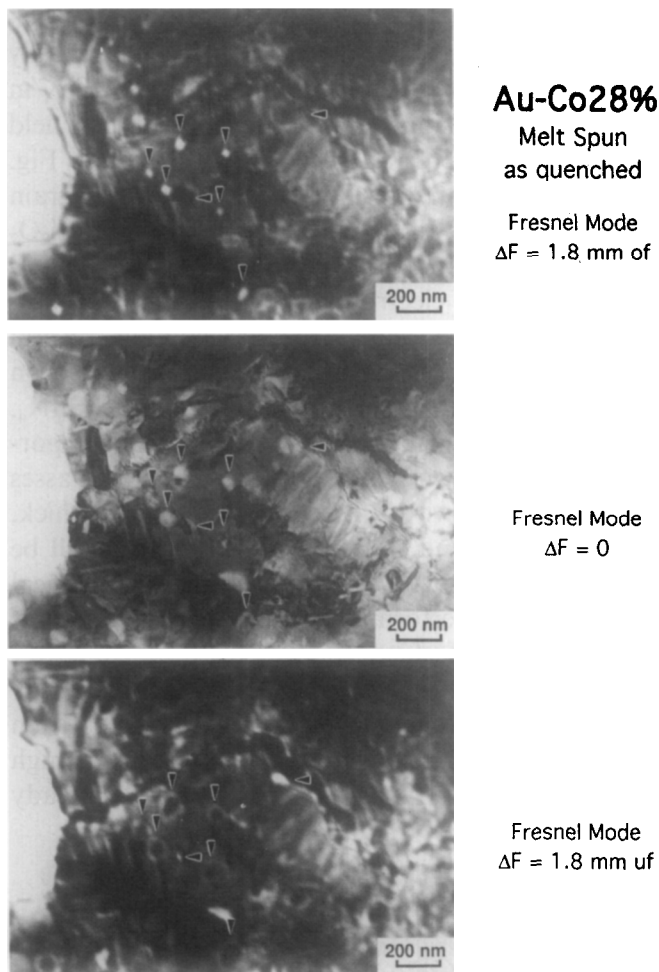


Fig. 13. Au 28at%Co alloy as quenched and imaged at 800 kV (in Berkeley ARM) in the diffraction mode. The arrows show changes in contrast for particles with similar direction of magnetization, and the central figure ($\Delta f = 0$) shows the particles with no magnetic contrast (courtesy J. Bernardi).

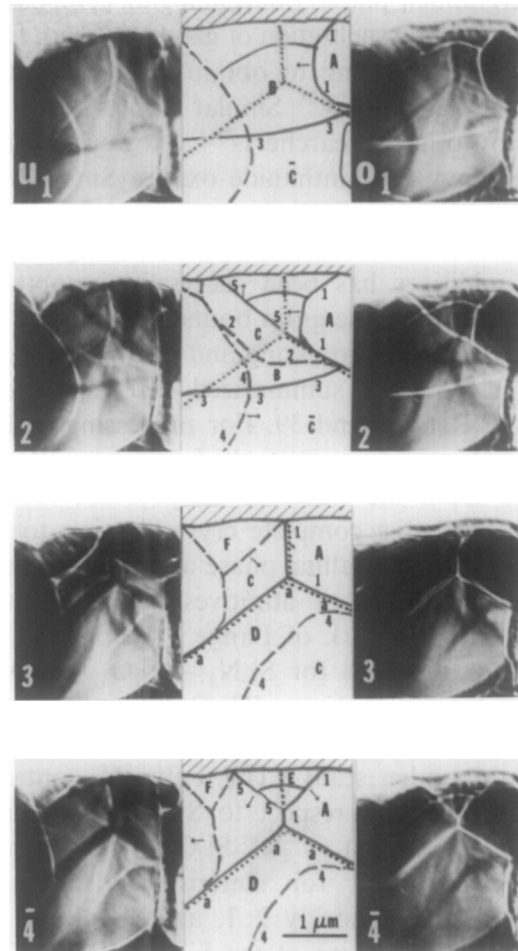


Fig. 14. MnZn ferrites Lorentz imaging for under- and over-focused conditions. Center column is sketch to indicate how grain boundary regions pin magnetic domain walls. The effective field is changed by specimen tilt. A large field reversal is needed to release the domain walls, hence decreasing permeability (Ref. 22).

tion, viscosity, etc. can deteriorate mechanical properties. A basic understanding of such intergranular and interphase interfaces is therefore essential if improvements in performance are to be

achieved. A program towards this end has been under way at Berkeley for some 15 years. In the course of this program, techniques were developed for high resolution electron optical characterization

Some Generic Microstructures: Ceramics

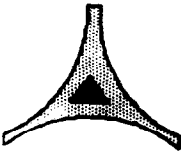

Grain boundaries / interfaces	Examples	Properties limited
	Amorphous films	Creep
	Partly crystalline films	Creep
	Additives / impurities	Permeability
		Voltage drop required
	Si_3N_4	Na^+ conduction
	Some Sialons	Conduction a-b plane
	Ferrites	Affects T_c and J_c
	Varistors	Varied (creep, etc.)
	β Na alumina	
	$\text{YBa}_2\text{Cu}_3\text{O}_{7-x}$	
	$\text{Bi}_2\text{Sr}_2\text{Cu}_n\text{Ca}_{n-1}\text{O}_y$	
	polytypoids of low T_c	
	ZrO_2 / mullite	
	composites	

Fig. 15. Schematic to indicate importance of grain boundaries and interphases on many properties of ceramics.

of intergranular phases (morphologies, composition), studies^{24–26} of crystallization of glasses^{27–29} and, finally, successful processing to obtain mostly crystalline intergranular phases.²⁸ Similar efforts have been made by other researchers.^{29–37} However, the use of the heavy RE lanthanide oxides (Sm→Tb) has received little attention outside our current research. In all materials studied, sintering with RE oxide additives has been successful in obtaining $\text{RE}_2\text{Si}_2\text{O}_7$ crystalline grain boundary phases.^{37–40}

The materials processing and testing procedures used in the work summarized here are given in detail in Refs 38 and 39. For processing with the rare-earth oxides, controlled cooling through 1400°C from the sintering temperature (1600°C) results in almost complete crystallization to form the $\text{RE}_2\text{Si}_2\text{O}_7$ crystalline phase at the grain boundaries. The choice of additives is based on the phase diagram work of Lange.³⁰ We assume that the phase relations for $\text{Si}_3\text{N}_4 - \text{Y}_2\text{O}_3 - \text{SiO}_2$ are similar to the $\text{Si}_3\text{N}_4 - \text{RE}_2\text{O}_3 - \text{SiO}_2$ systems, where RE represents Y, Sm, Gd, Dy, Er, and Yb, currently under study. The only RE-containing phase stable with respect to SiO_2 (the oxidation product of Si_3N_4) is $\text{RE}_2\text{Si}_2\text{O}_7$. The ratios of $\text{SiO}_2:\text{RE}_2\text{O}_3$ used for sintering aids to form $\text{RE}_2\text{Si}_2\text{O}_7$ are obviously 2:1, and a volume fraction of ~0.2, as given at the $\text{Si}_3\text{N}_4 - \text{RE}_2\text{Si}_2\text{O}_7$ tie line, is chosen so as to 'cover' all grain boundaries. Previous researchers have used $\text{Y}_2\text{O}_3 - \text{Al}_2\text{O}_3$ sintering aids,²⁹ but later work^{27,28} indicated that the glassy phase was stabilized by partitioning of Al and N during crystallization.

Figures 16 and 17 show electron micrographs of the sintering products using $\text{Yb}_2\text{O}_3 + \text{SiO}_2$. High aspect ratio grains of Si_3N_4 are surrounded by intergranular pockets (dark contrast in Fig. 16(a), (b)) of crystalline $\text{RE}_2\text{Si}_2\text{O}_7$ phase. These high

aspect ratio matrix grains are important in crack deflection, and such materials gave reasonably good K_{IC} fracture toughness values, e.g. ~8 $\text{MPa}\sqrt{\text{m}}$ in compact tension tests.⁴¹ The diffuse dark field image in Fig. 15(d) and the HREM image in Fig. 16 show that some residual glass remains at grain boundaries, and at the interfaces between $\text{RE}_2\text{Si}_2\text{O}_7$ crystal phases and Si_3N_4 at triple points. Preliminary analytical electron microscopy (AEM) indicates that these glassy regions contain several cationic impurities, notably Ca,²⁴ and research on this is continuing.⁴² Impurities (from the Si_3N_4 , SiO_2 , and RE_2O_3 starting powders) play an important role in glass retention. Although such glasses are often only two to three molecular layers thick, their viscosity and thus composition could still be the limiting factor in high temperature mechanical behavior and performance. In only rare instances are glass-free interfaces found,⁴⁰ e.g. Fig. 18. Auger and sputtering experiments on Si_3N_4 and AlN show that oxide layers form very quickly (within seconds) on the surface after removal from high vacuum. Thus, it may be that powders already

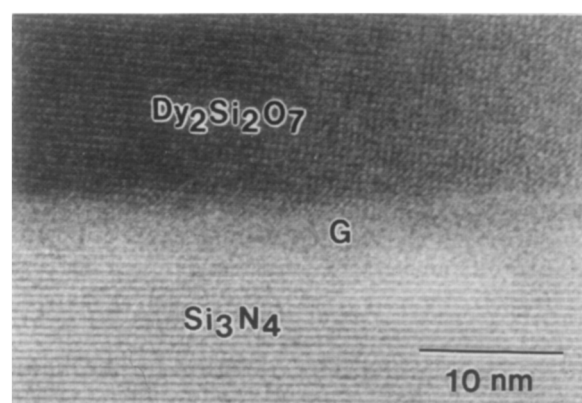


Fig. 17. Lattice image of $\text{Si}_3\text{N}_4 - \text{Yb}_2\text{O}_3$ sintered sample showing intergranular amorphous phase (Ref. 40).

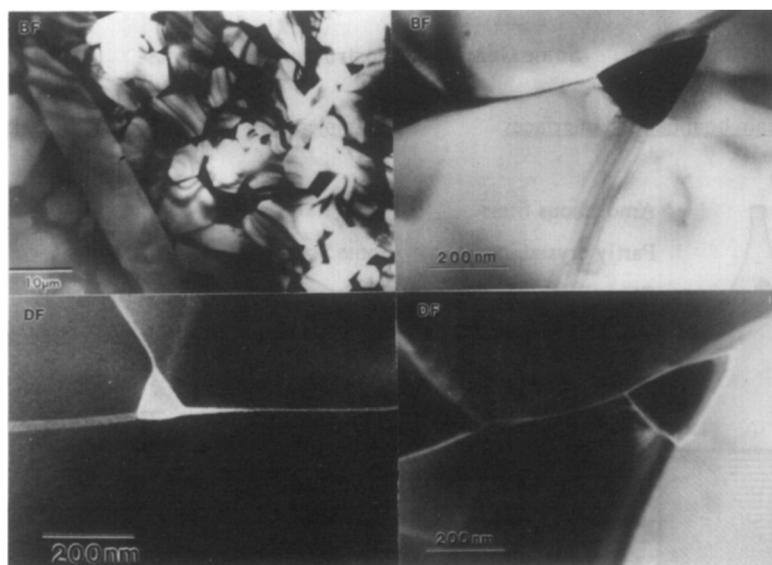


Fig. 16. Electron microscopy analyses of intergranular phases, crystalline and amorphous, in Si_3N_4 sintered with Yb_2O_3 (Ref. 40). Lower left is dark field image of RE silicate phase, lower right is diffuse dark field imaging showing glassy phase at grain boundaries.



Fig. 18. Lattice imaging showing a rare case of a glass-free $\text{Si}_3\text{N}_4/\text{Si}_3\text{N}_4$ interface (Ref. 40).

contain surface oxide, which on processing react to form intergranular monolayer glassy films.

These results of sintering silicon nitride with heavy rare-earth oxides to produce stable $\text{RE}_2\text{Si}_2\text{O}_7$ crystalline phases at grain boundaries are very encouraging. A summary of the main results obtained to date is given in Fig. 19. Sintering with $\text{RE}_2\text{Si}_2\text{O}_7$ produces material at nearly 99% theoretical density with a crystalline intergranular phase. Figure 19³⁸⁻⁴⁰ shows that these ceramics have greatly improved high temperature strength, creep and oxidation resistance. Results of fatigue behavior, Fig. 19(d), show no detrimental effects of the intergranular crystalline phase on fatigue behavior, probably because there is nearly always a glassy interface present.⁴¹ It is these interfaces that favor preferred crack propagation paths in both stable and fast fracture. Thus, the immediate crack tip environment may not be much affected by crystallization of the bulk intergranular phases. Greater differences are expected for high temperature testing where glasses become 'fluid.' The research is continuing, with emphasis on optimizing the sintered microstructures and more controlled fatigue experiments, especially at high temperatures. A detailed statistical survey of grain boundary films by HREM and AEM by Kleebe *et al.*⁴² showed that the glassy phase thickness at grain boundaries in Si_3N_4 sintered with Yb_2O_3 , Al_2O_3 and CaO depends on film chemistry. More work still is needed, however, especially high resolution microanalysis (including EELS).

3.2 Magneto-optical garnet heterostructures

The huge effort put into the development of a green-blue range diode laser has been coupled lately with a sustained effort in the study and production of magneto-optical (MO) materials that

respond to the blue radiation.⁴³ The MO materials already on the market are amorphous Tb-Fe-Co films with a decent response in the infrared region of the EM spectrum. Their response dies fairly quickly with an increase in radiation frequency. The idea behind the reduction of the wavelength is the increase in storage density (bit size is dependent on the resolution of the writing laser focused spot, which in turn is diffraction limited, controlled by the wavelength). By the end of the year, the thermo-magneto-optical media are expected to have about 25% of the optical memories market (reaching production of 12 million disks with a profit of \$300 million⁴³). The impact on the computer/memory industry is expected to increase when comparing the 10^8 bits/cm² of the MO disks with the 10^6 bits/cm² of the magnetic systems.

The best candidates considered for the next generation of MO materials are the garnets (particularly Bi substituted iron garnets; Bi increases the Faraday rotation), the ferrites, and the Co/Pt multilayers.⁴⁴ Of these, the garnets have the highest MO response in the blue-green range (our films have up to 54000 deg/cm in normal incidence reflective Faraday measurements).

Our effort has concentrated on the development of epitaxial heterostructures in collaboration with Belcore and IBM's Almaden Laboratory. Heterostructures of Bi-Fe-garnet and Y-Fe-garnet (BIG/YIG) as well as Eu-Bi-Fe-garnet and Y-Fe-garnet (EBIG/YIG) have been grown by pulsed laser ablation.⁴⁵ Experiments performed up to the present indicate increased MO performance and coercivities (up to 1.2 kOe for some films) with higher EBIG content of the films, as well as in improved MO response with a decrease of the total thickness of the films. The thick films (1.3–2.4 μm) showed rotations up to 13000 deg/cm, while the thin films (0.3–0.9 μm) go up to 54000 deg/cm. The increased performance of the thinner films raises the suggestion that magnetic coupling of the EBIG layers occurs through the YIG layers. The addition of Eu to the BIG structure has shown a change in the anisotropy of the films from in-plane to out-of-plane (all MO systems use perpendicular anisotropy for increased density and improved MO responses from the media).

Initial work by HREM-TEM indicates that while the YIG layers tend to grow epitaxially on the Gd-Ga-garnet (GGG) substrates (with high coherence of the interface, e.g. Fig. 20), the next layer (EBIG), although maintaining the apparent coherency, has to develop microstructural defects to accommodate the lattice mismatch with the YIG layer. Figure 21 is an example. Because the stresses induced in the material by the lattice mismatch tend to increase with the thickness of the layers,

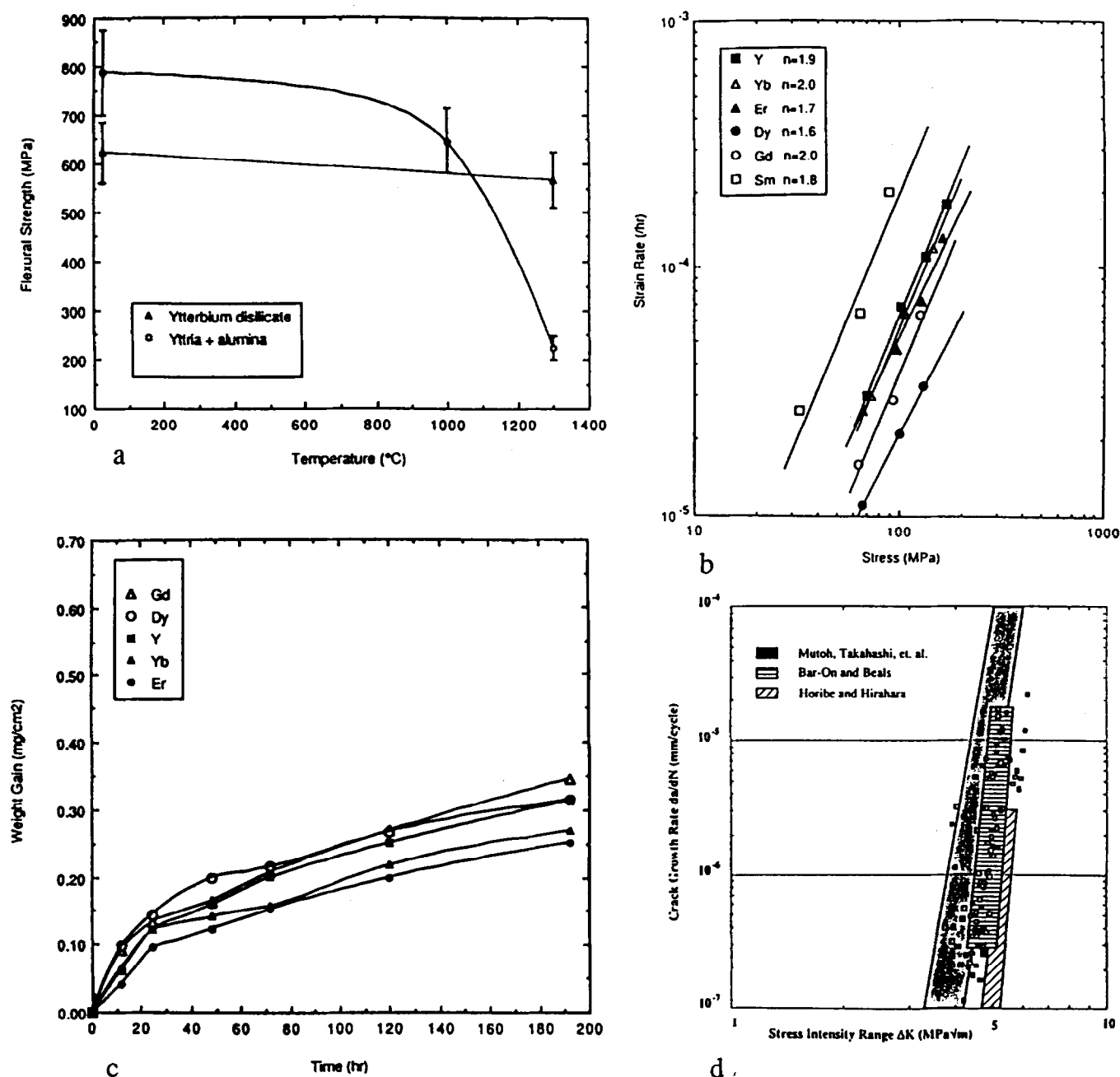


Fig. 19. Composite showing main mechanical properties of sintered Si_3N_4 : (a) Plot of flexural strengths from 25 to 1300 $^{\circ}\text{C}$; note the improvement for the Yb_2O_3 sintered material (Ref. 38; courtesy *J. Am. Ceram. Soc.*); (b) plot of steady state creep strain rates with applied stress at 1400 $^{\circ}\text{C}$ in air. The exponents are shown in the inset (Ref. 38; courtesy *J. Am. Ceram. Soc.*); (c) plot of oxidation rates (weight gain) at 1400 $^{\circ}\text{C}$ (Ref. 39; courtesy *J. Am. Ceram. Soc.*); (d) fatigue crack growth data for $\text{RE}_2\text{Si}_2\text{O}_7\text{-Si}_3\text{N}_4$ samples (data points) compared to published data (shaded) for room temperature tests; shows very little difference in crack growth rates (Ref. 41; courtesy Acta Met Inc.).

the thin films are probably prone to lower densities of such microstructural defects, and this may lead to improved MO responses. Such a relationship is speculative at this point and has to be proven by systematic microstructural characterizations of all the films in the series, followed by a coupling of these data with the magnetic and MO properties.

3.3 Multilayer mirrors: X-ray optics and interface roughness

The interest in multilayer mirrors in the soft X-ray regime is mainly twofold: (1) for X-ray lithography for digital devices requiring finer features and (2)

for X-ray microscopy for studying living biological specimens at high resolution. Such multilayers consist of alternating films of low density and high density materials, e.g. glass and heavy metal. The thickness of the layers is ideally quarter-wave-lengths so as to optimize the reflected intensity. The roughness of the interface is important in affecting X-ray reflectivity and intensity.⁴⁶ Figure 22 is an example for Mo/SiO_2 formed by magnetron sputtering using two fixed guns and a rotating substrate holder. It can be seen that the metal layer is very defective. Stress relaxation can occur by elastic/plastic/fracture mechanisms. In

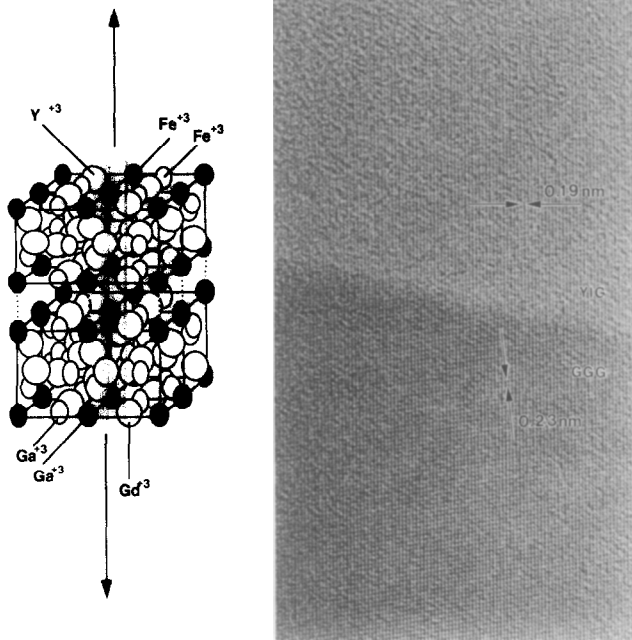


Fig. 20. Half unit cell diagrams indicating the substrate (GGG)/film (YIG) interface, and a high resolution image showing a GGG/YIG interface. The coherence of the interface indicates epitaxial growth. The image is taken in the $[-1 \ -5 \ 3]$ zone axis. The lattice spacings indicated correspond to one (026) plane - 0.19 nm and one (510) plane - 0.23 nm.

this case microtwinning can be resolved, and such twins produce surface shear steps which contribute to roughness during or after sputtering and can be independent of the smoothness of the substrate.

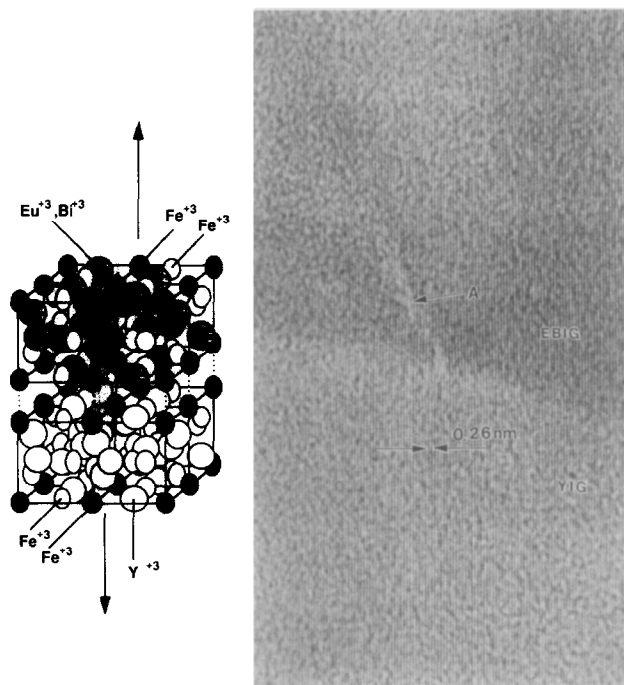


Fig. 21. Half unit cell diagrams indicating the template (YIG)/film (EBIG) interface, and a high resolution image showing a YIG/EBIG interface. The coherence of the interface indicates epitaxial growth. At this second interface a number of defects can be observed (A). The image is taken in the $[-1 \ -5 \ 3]$ one axis. The lattice spacing indicated corresponds to (224) planes. The lattice mismatch between the two films is of 0.96%.

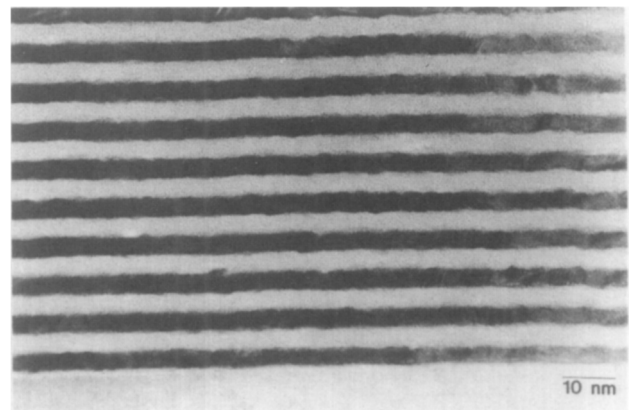


Fig. 22. Multilayer SiO_2/Mo films formed by magnetron sputtering. Notice high defect density in the Mo layers leading to interfacial roughness (courtesy C. Walton).

3.4 Multilayer magnetic oxides: roughness and coupling

Interfacial roughness is also an important factor which can affect electronic and magnetic properties. One example is ferromagnetic-antiferromagnetic coupling, which is effective in improving signal recording (noise reduction) in recording systems. One such system being studied in our group, in collaboration with Professor A. E. Berkowitz of U.C. San Diego,⁴⁷⁻⁴⁹ is coupling between ferromagnetic permalloy and antiferromagnetic NiO/CoO. The latter can be grown as a CoO-NiO alloy or multilayered NiO/CoO superlattices by sputtering on a suitable substrate, e.g. $\alpha\text{-Al}_2\text{O}_3$ [0001], to achieve [111] epitaxial growth.

As the schematic diagram of Fig. 23 shows, steps at the interface can interfere with the magnetic coupling. In addition to the similar task for preparing smooth multilayers for X-ray optics, the films must not deform plastically or else twin/slip steps are generated and rough interfaces can develop during or subsequent to film growth. Clearly, a study needs to be made of the accommodation of these films to strains, e.g. in terms of orientation, epitaxy, thickness, and heat treatment. Of course steps in the substrate surface can be propagated into the growing layer(s), so this first layer must be atomically smooth and clean to start.

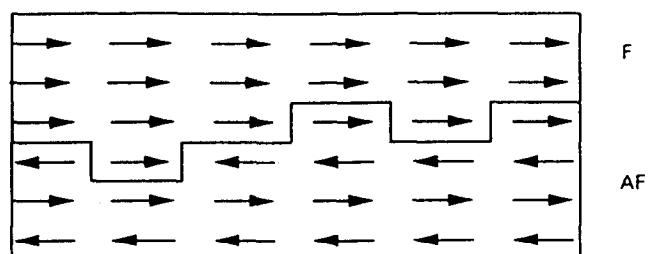


Fig. 23. Schematic of antiferromagnetic/ferromagnetic coupling. Notice now the roughness of the interface can affect the magnetic spin orientations and hence their interactions.

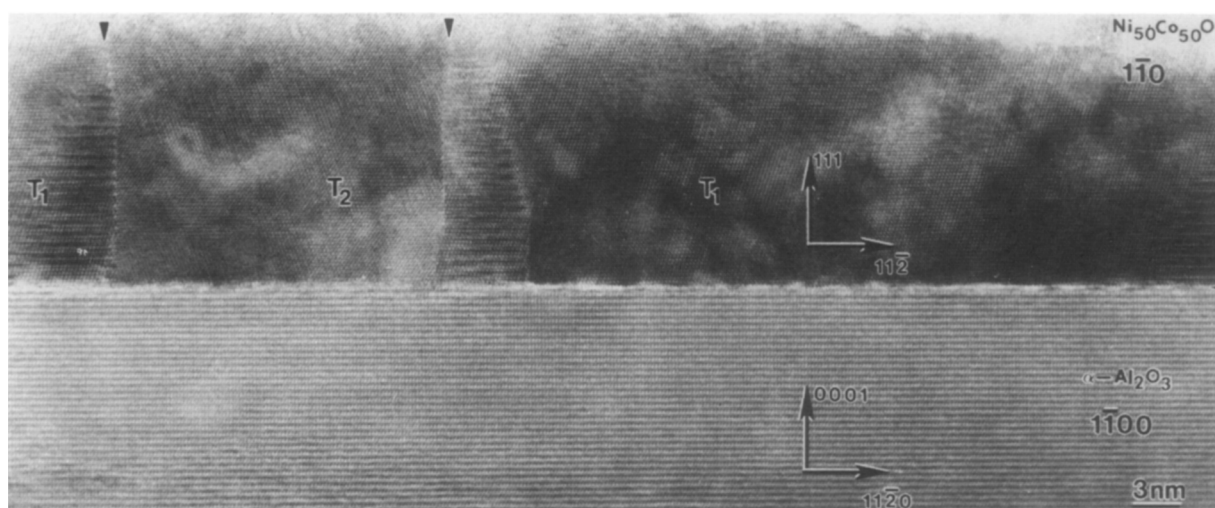


Fig. 24. Cross-section showing high resolution image of the epitaxial interface for CoONiO alloy sputtered onto [0001], α -Al₂O₃. Notice twins in the antiferromagnet (Ref. 47).

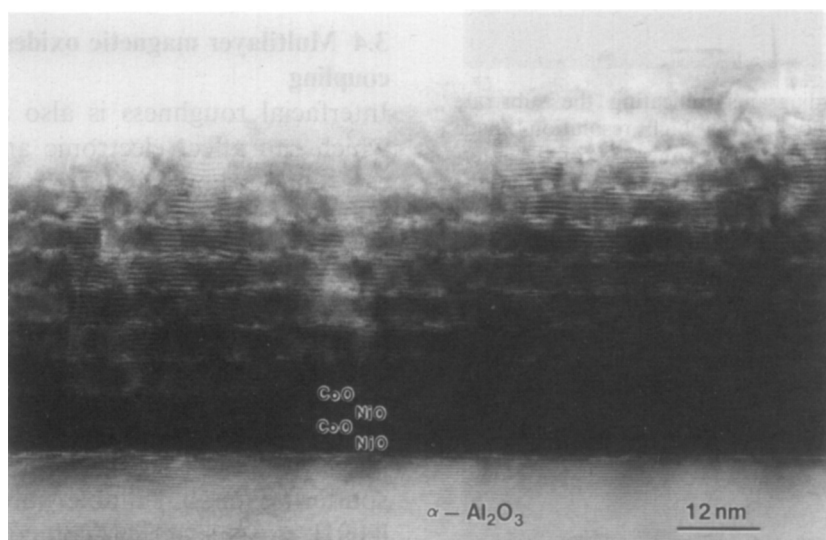


Fig. 25. Similar to Fig. 24 but with CoO/NiO multilayer sputtering. The CoO shows defect structures but no twins (Ref. 48).



Fig. 26. Cross-section of NiO/CoO and Fe/Ni interface which is very rough, resulting in poor magnetic coupling (courtesy W. Cao).

Figures 24 and 25 show these interfaces and Fig. 26 shows a poor permalloy–NiOCoO coupled interface.

4 Summary

Modern electron optical diffraction and analytical techniques are essential to understand ceramic (and *all*) materials. A major characterization difficulty is that of high resolution light element analysis, but ARM and PEELS hold great promise. Nevertheless, it is not too difficult to design ideal structures for specific property performance. The real challenge is the task of processing and consistent economical manufacturing practices, in order to produce the desired microstructures.

Acknowledgements

The research on magnetic recording materials is partially supported by National Science Foundation Grant No. DMR-90-10908 under a joint program with the Center for Magnetic Recording Research, University of California at San Diego (Professor A. E. Berkowitz). The work on structural ceramics and the electron microscopy facilities at the National Center for Electron Microscopy, Lawrence Berkeley Laboratory, are supported by the Director, Office of Basic Energy Sciences, Division of Materials Sciences of the United States Department of Energy under Contract No. DE-AC03-76SF00098. Work at Belcore/University of Maryland is supported by the Office of Naval Research. We acknowledge the cooperation of many groups, especially Professor R. Ramesh (Belcore and now University of Maryland), Dr. J. Petrovic at Los Alamos National Laboratory (MoSi₂), Mr Y. Goto of Toshiba (Si₃N₄ fibers), Dr E. Marinero (IBM Almaden Laboratory, San Jose, California), members of my research group, and co-authors of many of the examples cited in this short review.

References

1. Thomas, G., Electron Microscopy and materials science. *Acta Microscop.*, **1** (1) (1992) 1–19.
2. Spence, J. C. H., *Experimental High Resolution Electron Microscopy*, 2nd ed., Oxford University Press, UK, 1988.
3. Epicer, T., O'Keefe, M. A. & Thomas, G., Atomic imaging of 3:2 mullite. *Acta Cryst.*, **A46** (1990) 948–62.
4. See, for example, the annual proceedings of the Microscopy Society of America, and the proceedings of the International and Regional Electron Microscopy Congresses held every four years.
5. For example, M. O'Keefe, National Center for Electron Microscopy, Lawrence Berkeley Laboratory, Berkeley, California 94720, USA.
6. Steeds, J. W., Convergent beam electron diffraction. In *Introduction to Analytical Electron Microscopy*, eds J. J. Hren, T. J. Goldstein & D. C. Joy, Plenum, New York, 1979, pp. 387–422.
7. Dass, M. L. A., Bielicki, T. A. & Thomas, G., Convergent beam studies on lead zirconate titanate ceramics. In *Proceedings of the Electron Microscopy Society of America*, ed. G. W. Bailey. San Francisco Press, 1986, pp. 482–3.
8. Callahan, D. L. & Thomas, G., Convergent beam diffraction analysis of lattice shifts in AlN. *J. Am. Ceram. Soc.*, **75** (5) (1992) 1092–6.
9. Thomas, G. & Goringe, M. J., *Transmission Electron Microscopy of Materials*, J. Wiley & Sons, New York, and Tech Books, Fairfax, VA, 1981.
10. Merk, N. & Thomas, G., Structure and composition of submicroscopic mullite whiskers. *J. Mat. Res.*, **6** (4) (1991) 825–34.
11. Epicer, T. A., Wohlfromm, H. & Thomas, G., Dislocation analysis in Al₂TiO₅. In *Proceedings of the Electron Microscopy Society of America*, ed. G. W. Bailey. San Francisco Press, 1989, pp. 422–3.
12. Van Tendeloo, G., Faker, K. T. & Thomas, G., Characterization of long period polytypoids in AlN ceramics. *J. Mat. Sci.*, **18** (1983) 525–7.
13. Krishnan, K. M., Rai, R. S., Thomas, G., Corbin, N. D. & McAuley, J. W., Characterization of long period polytypoids in Al₂O₃–AlN System. In *Mat. Res. Soc. Symp. Proc.*, **60** 1986, pp. 211–20.
14. Shaw, T. M. & Thomas, G., Electro microscopy study of Be₃N₂–BeSiN₂ systems. *J. Sol. State Chem.*, **33** (1) (1980) 63–82.
15. Ramesh, R., Green, S. M. & Thomas, G., Microstructure property relationships in ceramic superconductors. In *Studies of High Temperature Superconductors*, Vol. 5, ed. Anant Narlikar. New York, Nova Science Publishers (4) 1989, pp. 361–403.
16. McFayden, André, Mullite-whisker reinforced molybdenum disilicide composites. PhD thesis. University of California, Berkeley, CA, 1995.
17. Vasudevan, A. K. & Petrovic, J. J., A comparative overview of molybdenum disilicide composites. *Mater. Sci. Eng.*, **A155** (1992) 1–17.
18. Lessing, P. A., Gordon, R. S. & Mazdiasni, K. S., Creep of polycrystalline mullite. *J. Am. Ceram. Soc.*, **58** (1975) 149.
19. Williams, D. B., *Practical Analytical Electron Microscopy in Materials Science*, Verlag Chemie Int., 1984.
20. Blake, D. F. *et al.* Nature and origin of interstellar diamond. *Nature*, **332** (1988) 611–13.
21. *Proceedings of Symposium on Magnetic Imaging*, Microscopy Society of American, eds G. W. Bailey & C. L. Rider, San Francisco Press, 1993, pp. 1010–53.
22. Lin, I-Nan, Mishra, R. K. & Thomas, G., TEM study of structure and composition of MnZn ferrites. In *Proceedings of Advanced Materials Characterization*, Plenum, New York, 1983, pp. 351–8.
23. Thomas, G., High resolution analyses and interfacial design of inorganic materials. *Scripta Metall Mater.*, **31** (1994) 953–8.
24. Clarke, D. R. & Thomas, G., Microstructure of Y₂O₃ fluxed hot pressed silicon nitride. *J. Am. Ceram. Soc.*, **61** (1978) 114–18.
25. Thomas, G., Grain boundaries and interfaces. In *Ceramic Microstructures '86*, eds J. A. Pask & A. G. Evans. Plenum, New York, 1988, pp. 55–72.
26. Thomas, G., Ahn, C. & Weiss, J., Characterization and crystallization of Y–Si–Al–O–N glasses. *J. Am. Ceram. Soc.*, **65** (1982) C185–8.
27. Dinger, T. R., Rai, R. S. & Thomas, G., Crystallization behavior of a glass in the Y₂O₃–SiO₂–AlN system. *J. Am. Ceram. Soc.*, **71** (1988) 236–44.
28. Cinibulk, M. K., Thomas, G. & Johnson, S. M., Fabrication and secondary phase crystallization of RE disilicate–Si₃N₄ ceramics. *J. Am. Ceram. Soc.*, **75** (1992) 2037–43.

29. Tsuge, A., Nishida, K. & Komatsu, M., Effect of crystallizing grain boundary phase on high temperature strength of hot pressed Si_3N_4 ceramics. *J. Am. Ceram. Soc.*, **58** (1975) 323–6.
30. Lange, F. F., Singhal, S. C. & Kuznicki, R. C., Phase relations and stability studies in Si_3N_4 - SiO_2 - Y_2O_3 pseudoternary system. *J. Am. Ceram. Soc.*, **60** (1977) 249.
31. Loehman, R. E., Preparation and properties of oxynitride glasses. *J. Non-Cryst. Solids*, **56** (1983) 411–16.
32. Clarke, D. R., Lange, F. F. & Schnittgrund, G. D., Strengthening of sintered Si_3N_4 by a post-fabrication heat treatment. *J. Am. Ceram. Soc.*, **65** (1982) C51–2.
33. Bonnell, D. A., Tien, T.-Y. & Rühle, M., Controlled crystallization of the amorphous phase in silicon nitride ceramics. *J. Am. Ceram. Soc.*, **70** (1987) 460–5.
34. Cinibulk, M. K., Thomas, G. & Johnson, S. M., Grain boundary phase crystallization and strength of Si_3N_4 sintered with YAlSiO_3 glass. *J. Am. Ceram. Soc.*, **73** (1990) 1606–14.
35. Sanders, W. A. & Mieskowski, D. M., Strength and microstructure of sintered Si_3N_4 with RE oxide additions. *J. Am. Ceram. Soc.*, **64** (1985) 304–9.
36. Lewis, M. H., Reed, C. J. & Baker, N. D., Pressureless sintered ceramics based on $\text{Si}_2\text{N}_2\text{O}$. *Mat. Sci. Eng.*, **71** (1985) 87–94.
37. Wiederhorn, S. M. & Tighe, J. J., Structural reliability of Y_2O_3 doped hot pressed Si_3N_4 at elevated temperatures. *J. Am. Ceram. Soc.*, **66** (1983) 884–9.
38. Cinibulk, M. K., Thomas, G., & Johnson, S. M., Strength and creep behavior of RE disilicate – Si_3N_4 ceramics. *J. Am. Ceram. Soc.*, **75** (1992) 2050–5.
39. Cinibulk, M. K., Thomas, G. & Johnson, S. M., Oxidation behavior of RE disilicate – Si_3N_4 ceramics. *J. Am. Ceram. Soc.*, **75** (1992) 2044–9.
40. Goto, Y. & Thomas, G., Microstructure of Si_3N_4 ceramics sintered with RE oxides. *Acta Metall. Mater.*, **43** (1995) 923–30.
41. Cornelissen, B. E., Dauskart, R. H., Ritchie, R. O. & Thomas, G., Cyclic fatigue behavior and fracture toughness of Si_3N_4 ceramics sintered with RE oxides. *Acta Metall. Mater.*, **42** (1994) 3055–64.
42. Kleebe, H.-J., Cinibulk, M. K., Cannon, R. M. & Rühle, M., Statistical analysis of the intergranular film thickness in silicon nitride ceramics. *J. Am. Ceram. Soc.*, **76** (1993) 1969–77.
43. Hall, C. W., Magneto-optic media. In *Storage and Recording Systems*, Conference Publication 402. London, Institute of Electrical Engineers, 1994, pp. 137–9.
44. Lin, C. J., Co/Pt multilayers for magneto-optical recording. In *High Density Recording*, ed. K. H. J. Buschow, NATO ASI Series, 1993, pp. 461–81.
45. Simion, B. M., Ramesh, R., Keramidas, V. G., Pfeffer, R. L., Thomas, G. & Marinero, E., Magnetic characterization of epitaxial $\text{Y}_5\text{Fe}_3\text{O}_{12}/\text{Bi}_3\text{Fe}_5\text{O}_{12}$ and $\text{Y}_5\text{Fe}_3\text{O}_{12}/\text{Eu}_1\text{Bi}_2\text{Fe}_5\text{O}_{12}$ heterostructures grown by pulsed laser deposition. In *Epitaxial Oxide Thin Films and Heterostructures*, eds D. K. Fork, J. M. Phillips, R. Ramesh & R. M. Wolf, Pittsburgh, *Mat. Res. Soc.*, 1994, pp. 65–72.
46. Hütten, A., Cao, W., Walton, C. & Thomas, G., Structural properties of multilayer thin films. In *Proceedings of 13th Congress on Electron Microscopy*, 2A, Paris, French Society for Electron Microscopy, 1994, pp. 231–2.
47. Cao, W., Thomas, G., Carey, M. J. & Berkowitz, A. E., Characterization of epitaxially sputtered $\text{Ni}_x\text{Co}_{1-x}$ thin films on $\alpha\text{-Al}_2\text{O}_3$ using TEM. *Scripta Metall. Mater.*, **25** (1991) 2633–8.
48. Carey, M. J., Spada, F. E., Berkowitz, A. E., Cao, W. & Thomas, G., Preparation and structural characterization of sputtered CoO/NiO thin epitaxial films. *J. Mat. Res.*, **6** (1991) 2680–7.
49. Fullerton, E. E., Cao, W., Thomas, G., Schuller, I. K., Carey, M. J. & Berkowitz, A. E., Quantitative characterization of epitaxial superlattices by X-ray diffraction and HREM. *Appl. Phys. Lett.*, **63** (1993) 482–8.